Characterization of coal combustion products using variable rate CPT in a geotechnical centrifuge

Jiarui Chen[1#], and *Alejandro* Martinez[1]

[1]*University of California, Davis, Department of Civil and Environmental Engineering, One Shields Avenue, Davis, CA 95616, USA*
[#]*Corresponding author: jrcchen@ucdavis.edu*

ABSTRACT

Characterizing the in-situ state of soils is essential for evaluating their vulnerability and the consequences of failure. The cone penetration test (CPT) enables efficient, repeatable, and continuous soil characterization based on the recorded response to penetration. Particularly for waste storage facilities, analysis of CPT results can help avoid failures that could lead to significant socio-economic and environmental impacts. Human-made soils in waste storage facilities, like coal combustion products and mine tailings, can have a large fraction of silt-sized particles, which makes them prone to experiencing partial drainage during CPT soundings at standard penetration rates. However, the current state of practice still predominantly adopts the assumption of fully drained or undrained conditions, which may lead to inaccurate interpretation of soil properties and state. This study aims to explore a new CPT-based characterization framework for intermediate silty soils using cone tip resistance values to determine the soil state. To do so, CPT soundings were performed in-flight in centrifuge models of a coal combustion product with different initial densities at varying penetration velocities. Soils with a low density and contractive behavior experience a decrease in tip resistance as the penetration velocity is increased due to the generation of excess pore pressures, resulting in high ratios of drained to undrained tip resistance $(Q_{tn,drained}/Q_{tn,undrained})$. In contrast, the tip resistance increases with penetration velocity, resulting in low $Q_{tn,drained}/Q_{tn,undrained}$ ratios in soils of a high density and dilative behavior. The proposed framework uses $Q_{tn,drained}/Q_{tn,undrained}$ to identify contractive layers and is expected to help assess the vulnerability of soil layers to experience liquefaction failure.

Keywords: cone penetration test; static liquefaction; characterization; silty soil.

1. Introduction

Identifying the risk of static liquefaction in intermediate or transitional soils, including coal combustion products (CCP) and mine tailings, has become increasingly important due to significant property damage and environmental impacts caused by multiple devastating flow liquefaction failures in the past 20 years, such as the 2008 Kingston Fossil Plant failure and the 2019 Brumadhino tailings dam failure. Cone penetration tests (CPT) are used routinely in geotechnical soil characterization to estimate soil properties and state and perform engineering analysis. However, the estimation of soil properties for soils with large fractions of silty particles like CCPs and mine tailings has more uncertainty than for sands and clays due to the potential partial drainage conditions during soundings at the standard penetration rate of 20 mm/s per ASTM D5778-20. The current state of practice still predominantly adopts the assumption of fully drained or undrained conditions for the interpretation of CPT results in these intermediate problematic soils, which can lead to inaccurate estimation of soil state (DeJong and Randolph 2012). For example, Robertson (2010) provides an approach to estimate the initial state of the soil to the equivalent clean sand normalized cone tip resistance from CPTs ($Q_{tn,cs}$), which is a cone tip resistance under fully drained conditions. The developed correlation for converting the normalized cone tip resistance (Q_{tn}) to $Q_{tn,cs}$ accounts for the soil type only but does not directly account for the potential for partial drainage conditions. Shuttle and Jefferies (2016) developed a CPT-based interpretation framework using cavity expansion theory and a sophisticated soil constitutive model, Norsand. However, the calibration of the Norsand model requires additional input parameters from advanced laboratory tests as well as the assumption of drained or undrained conditions. Plewes et al. (1992) and Jefferies and Been (2015) take into account the excess pore water pressure generated at the u_2 position of the cone penetrometer (ASTM D5778-20) to adjust the normalized cone tip resistance. However, the empirical relationship was based on a limited database that excluded problematic intermediate soils like CCP materials or mine tailings. While these advances have improved in-situ characterization of soils, there is still a need for accurate CPT-based frameworks to assess the soil state of problematic intermediate soils to inform their susceptibility to failure. This study explored the development of such a framework based on centrifuge in-flight CPTs performed in fly ash models.

2. Testing materials

The CCP tested in the current study is the same fly ash material used by Madabhushi et al. (2023) and EPRI (2021) in centrifuge run-out tests. The material is classified as a Class-F fly ash, which is typically derived from bituminous and anthracite coals and consists primarily of an alumino-silicate glass with quartz, nullite, and magnetite. The ash's calcium content (i.e., CaO) is less than 10%. Additionally, when this fly ash is saturated with water, it exhibits no diagenesis. The plasticity index (PI) of the material is close to zero, and its liquid limit (L_L) is about 25%. Multiple grain size test results have been reported, as presented in Figure 1. In general, the fines content (FC) is over 90%, and the clay size fraction is about 5%; thus, the behavior of this soil is likely dominated by the silt-size particles. Oedometer tests indicate a vertical coefficient of consolidation (C_v) between 0.44 and 1.61 cm^2/s based on tests with pressures of up to 400 kPa. Additional information on the tested fly ash is presented in Table 1.

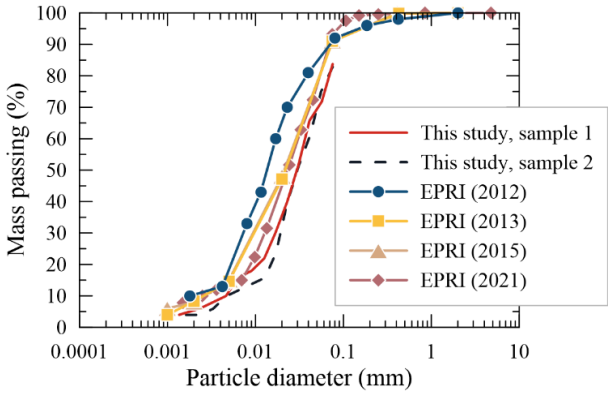

Figure 1. Grain size distribution of the tested CCP.

Table 1. Properties of tested fly ash

	EPRI (2012)	EPRI (2021)	This study
Specific gravity in water, G_s	2.28	2.54 – 2.56	2.44 – 2.47
10th percentile size, D_{10} (mm)	0.003	0.0025	0.0046
50th percentile size, D_{50} (mm)	0.014	0.024	0.030
Fines content, FC (%)	92	93	94
Clay size fraction (%)	10	9	5
Compression index, C_C	-	0.053	0.024 – 0.026
Vertical coefficient of consolidation, c_v (cm/s^2)	-	0.48 – 0.81	0.44 – 1.61

The critical state properties of the tested fly ash are of interest to characterize the state of the prepared fly ash model. Particularly, the locus of the critical void ratio (Casagrande 1936), usually termed the critical state line (CSL), needs to be determined. Isotropically consolidated undrained triaxial tests were performed to obtain the CSL, which can be represented using either of the following two equations (EPRI 2021), where the first one assumes a linear CSL in semi-log space and the second one uses a power function:

$$e_c = 1.540 - 0.25 \log p' \quad (1)$$

$$e_c = 1.284 - 0.29 \left(\frac{p'}{p_a}\right)^{0.23} \quad (2)$$

where, e_c is the critical void ratio, p' is the mean effective stress at the critical state, and p_a is the atmospheric pressure.

The state parameter, defined as the difference between the current (e) and the critical state void ratios at the same mean effective stress ($\psi = e - e_c$, Been and Jefferies 1985), is used in this investigation to characterize the volumetric change tendencies of the soil. The state parameter serves as a useful tool to infer whether the soil would exhibit contractive or dilative tendencies during shearing.

3. Centrifuge modeling

3.1. Centrifuge testing and experiment setup

The centrifuge tests were performed at an acceleration of 70-g at around one-third of the depth of the model in the 1-m radius centrifuge at the Centre for Geotechnical Modelling (CGM) at the University of California Davis (UC Davis). Throughout this paper, the dimensions and measurements are provided in prototype scale.

3.2. Sensors

Sensors, including capacitance moisture sensors, customized tensiometers/pore water pressure sensors, and bender elements, were placed against the inner sides of the CCP container (Figure 2). Particularly, the capacitance moisture sensor, model GS3 from the Meter Group Inc., was used to infer the gravimetric water content of the fly ash in-flight during and after consolidation. As shown in Figure 2 (a), four layers of sensors were placed in the saturated fly ash model to obtain measurements at different heights. Customized pore water pressure sensors/tensiometers constructed following the procedures outlined in Jacobsz (2018) with minor modifications were used to facilitate monitoring the consolidation progress of the fly ash during the increase of the g-level. The ceramic stones used for the pore water pressure sensor assembly had an air entry value of 300 kPa. Bender elements were also used to obtain the shear wave velocities (V_s) of the constructed model after primary consolidation.

3.3. Sample preparation

Saturated fly ash models were constructed to different initial void ratios. A layer of saturated Monterey #0/30 sand with a thickness of 2 cm was placed at the bottom of the container and compacted by hand. A layer of filter paper was placed on top of the sand to avoid the migration of fly ash particles. The fly ash was prepared using slurry deposition to replicate the in-situ deposition process. To minimize severe particle segregation during the deposition process (Dominguez-Quintans et al. 2023), the entire fly ash part was deposited in four lifts with an average thickness of about 4.5 cm to form a deposit with a total thickness of about 18 cm. Sufficient

time was allowed in between lifts to ensure the settlement of all particles.

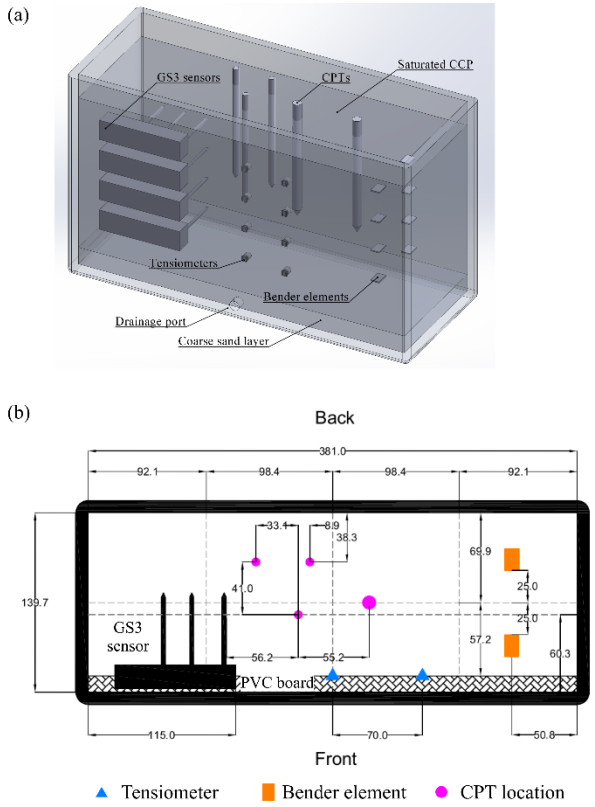

Figure 2. (a) Schematic of the sensor and CPT locations within the CCP container; (b) detailed plan view of the sensor and CPT locations within the CCP container (annotations in mm, bender elements, and tensiometers are not to scale).

Recent research successfully demonstrated that the slurry deposition technique produces loose specimens with strain-softening behaviors (Madabhushi et al. 2023; Reid et al. 2023) and dense, dilative specimens (Price et al. 2019; Riveros and Sadrekarimi 2021). The resulting density of the deposit can be controlled by adjusting the initial mixing water content of the slurry. As such, trials were performed to investigate the relationship between the initial and settled water contents, as shown in Figure 3. In general, the water content (or equivalently, the void ratio) of the settled fly ash increased as the water content of the slurry increased. For the tested material, slurry water contents from 30% to 400% led to settled water contents ranging from 20% to 60% (Figure 3), which correspond to void ratios between 0.502 and 1.506, calculated using a specific gravity of 2.51 and assuming full saturation.

Guided by the slurry deposition trials, centrifuge models were constructed using initial slurry water contents ranging from 35% to 240%. After sufficient settlement time, models with various water contents and void ratios were obtained (Table 2). The fly ash consolidated as the centrifuge was spun up to 70-g. The readings from the GS3 moisture sensor were used to back-calculate water contents and void ratios, which generally decreased due to in-flight consolidation (Table 2), resulting in initial water contents between 25.2% and 41.2%, corresponding to void ratios of 0.631 and 1.034. Even though the same initial slurry water content was used to create the 1-2 and 1-4 models, the consolidated water content differed due to the disturbance during loading the deposit on the centrifuge and spin up. Multiple spin-ups and spin-downs may need to be performed to achieve the centrifuge balance.

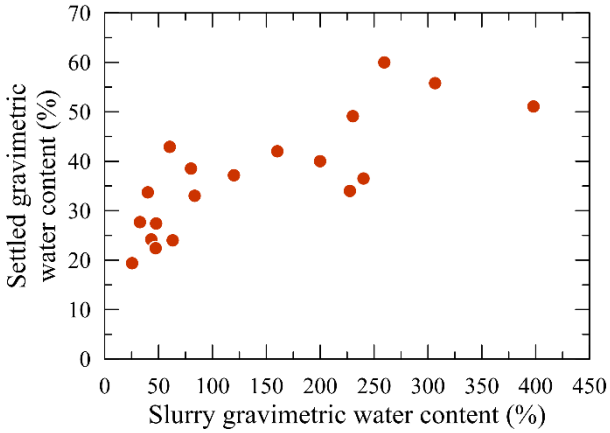

Figure 3. Relationship between the initial slurry gravimetric water content and the settled gravimetric water content.

Table 2. Summary of sample preparation conditions

Test No	Sample preparation			Consolidated condition[2]	
	Slurry	Settled[1]			
	w	w	e	w	e
	%	%		%	
1-1	35	29.6	0.743	25.2	0.631
1-2	240	41.9	1.052	41.2	1.034
1-4	240	41.9	1.051	30.9	0.775

Note: [1]the water content and void ratio after the soil particles are fully settled at 1-g; [2]back-calculated using the dielectric permittivity measurements from the moisture sensor.

3.4. Cone penetration testing

Four in-flight CPTs were performed in each fully saturated model deposit with various penetration rates. The CPT probes were only equipped to measure tip resistance, meaning that friction sleeve and pore pressure measurements were not obtained. Two miniature cone penetrometers with diameters (d) of 6 mm and 10 mm were used. The larger cone penetrometer was used to further increase the achievable normalized velocity (V) with the maximum penetration rate possible (v) in the centrifuge (i.e., 170 mm/s) since V is positively related to the cone diameter as follows (DeJong and Randolph 2012; Salgado 2014):

$$V = \frac{vd}{c_v} \tag{3}$$

In this study, a C_v = 0.6 cm^2/s was adopted based on the results from EPRI (2021). Based on Eq. (3), the calculated V spanned from 0.05 to 28.3, which was deemed sufficient to reach both drained and undrained conditions (DeJong and Randolph 2012). The CPT sounding locations are shown in Figure 2. A distance of at least six cone diameters between any two CPT locations and between the CPT location and the container sidewall was maintained to minimize disturbance and boundary effects. Additionally, the CPT locations were

also assigned outside of the volume of influence of the GS3 sensors to avoid any impact on the interpretation of gravimetric water content.

4. Test results and interpretation

4.1. Shear wave velocity results

Shear wave velocities were measured in all tested fly ash models to facilitate the characterization of the deposited soil. Bender elements were triggered at multiple g-levels after primary consolidation was completed. The obtained shear wave velocities are plotted against the effective vertical stress (σ'_{vo}) at the bender element locations in Figure 4. Despite the differences in the settled and consolidated model densities, the relationships between V_s and σ'_{vo} for all three deposits generally follow a single power-law curve with the form: $V_s = \alpha\ \sigma'^{\beta}_{vo}$. Regressed parameters are indicated in Figure 4. The parameters fall in the range reported for fly ash by published literature (Bachus et al. 2019). The good fit of the power-law function suggests that the V_s of the tested fly ash does not have a significant dependency on the density or void ratio.

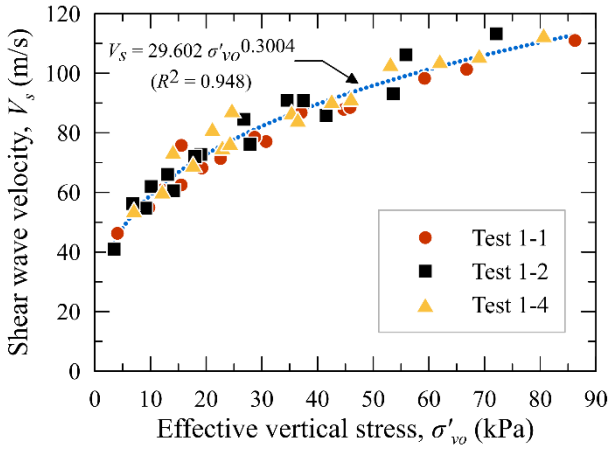

Figure 4. Relationship between shear wave velocity and effective vertical stress

4.2. Cone tip resistance profiles

The q_c readings in fully saturated soils are deemed essential to characterize the soil type and state (Robertson 2016) and quantify soil strength (Olson and Stark 2003). The CPT soundings for representative models Test 1-1 (densest) and Test 1-2 (loosest) are presented in Figure 5. In general, the q_c in the dense Test 1-1 increased with the penetration rates due to the generation of negative excess pore pressures, while the q_c in the loose Test 1-2 decreased due to the generation of positive pore pressures. These results indicate that the selected cone push rates lead to a wide range of drainage conditions.

All q_c profiles in the dense model (Test 1-1) generally increased with depth. In contrast, some layering appeared to exist in the loose model (Test 1-2), manifested by the fluctuation in the obtained q_c profiles with depth. However, despite the observed layering, a trend of the q_c profiles with the cone penetration rate could still be identified.

The overburden normalized cone tip resistance (Q_{tn}) is widely used in engineering practice instead of raw qc value because it allows the comparison of the strengths of soil at various depths and with different densities. Thus, the q_c profiles shown in Figure 5 were further processed to obtain Q_{tn} using the following equation (Robertson 2016):

$$Q_{tn} = \left(\frac{q_c - \sigma_{vo}}{p_a}\right)\left(\frac{p_a}{\sigma'_{vo}}\right)^n \quad (4)$$

$$n = 0.381 I_c + 0.05\left(\frac{\sigma'_{vo}}{p_a}\right) - 0.15 \quad (5)$$

where σ_{vo} is the total vertical stress and σ'_{vo} is the effective vertical stress. The saturated unit weight of the soil in each model was determined using the consolidated void ratio and the specific gravity. The water table height was back-calculated using the pore water pressure measurements at known locations. P_a is the atmospheric pressure, and the parameter n is a function of the soil type, which could be quantitatively represented using the SBTn soil behavior type index (I_c), which is defined as follows:

$$I_c = [(3.47 - \log Q_t)^2 + (\log F_r + 1.22)^2]^{0.5} \quad (6)$$

$$Q_t = \frac{q_c - \sigma_{vo}}{\sigma'_{vo}} \quad (7)$$

$$F_r = \frac{f_s}{q_c - \sigma_{vo}} \quad (8)$$

where F_r is the friction ratio, and f_s is the sleeve friction.

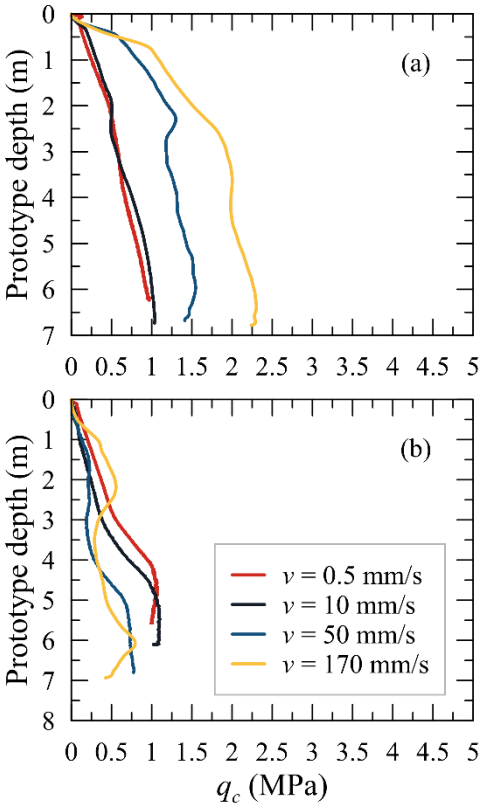

Figure 5. Cone tip resistance profiles under various penetration rates: (a) Test 1-1 (densest); (b) Test 1-2 (loosest).

As previously mentioned, the miniature cone penetrometers adopted in the current study were not equipped to obtain sleeve friction measurements. Instead, the correlation provided by Jefferies and Been (2015)

was used to calculate F_r based on the linear CSL slope (Eq. 1) in the semi-log space (λ_{10}) as follows:

$$F_r = 10\lambda_{10} \quad (9)$$

An λ_{10} of 0.25 from Eq. (1) leads to a F_r of 2.5%. The resulting Q_{tn} profiles are shown in Figure 6. Compared with the raw q_c profiles, where the cone tip resistance generally kept increasing due to the increase in σ'_{vo}, the Q_{tn} tends to be relatively constant (Figure 6 a) or show some variability with depth (Figure 6b). While the interpreted moisture content data along the model depths indicated a rather uniform gravimetric water content in loose models (e.g., Test 1-2), fluctuation in Q_{tn} indeed existed. The fluctuation in CPTs with various penetration rates generally happened at the same depth (Figure 6b), indicating none or negligible spatial variability horizontally. However, the fluctuation in the vertical direction will be explored more in future studies. Potential reasons may include layering within the model caused by the initially high slurry water content.

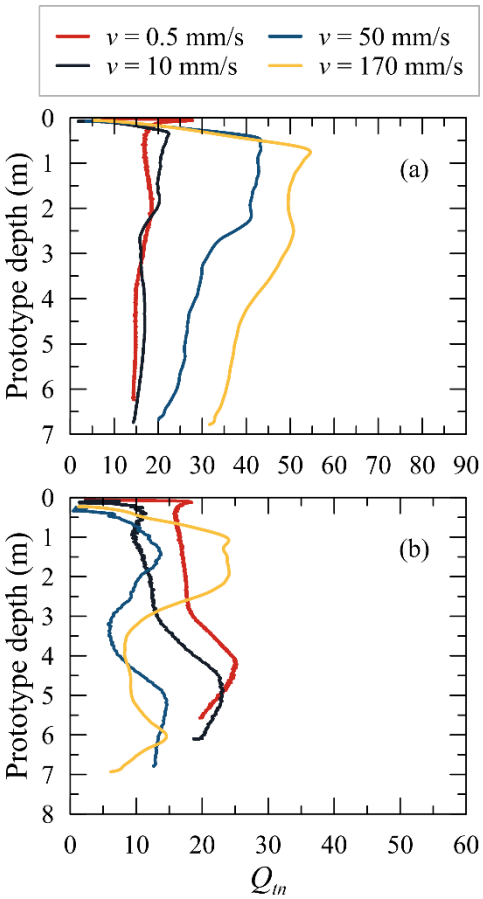

Figure 6. Interpreted normalized penetration resistance Q_{tn} profiles: (a) Test 1-1 (densest); (b) Test 1-2 (loosest).

4.3. Soil behavior type interpretation

The SBTn soil behavior type index (I_c) acts as an important soil characterization parameter for identifying the soil type, obtaining additional engineering parameters (e.g., the parameter that relates q_c to Standard Penetration Test blowcount N_{60}), and also assessing the vulnerability to potential geohazards. The I_c calculated using different penetration rates is shown in Figure 7 for the models in Test 1-1 and 1-2, which have the lowest and highest void ratios. In geotechnical engineering practice, I_c = 2.6 is considered an approximate boundary between soils that are either more sand-like or more clay-like (Robertson 2016). This threshold value (I_c = 2.6) was determined based on cyclic liquefaction case histories that were limited to predominately normally consolidated silica-based soils. It has been recognized that the circular shape of the I_c in $Q_t - F_r$ space is a less effective fit to the SBT boundaries, manifested as the fact that I_c = 2.6 lies within Zone 4 – silt mixtures (Robertson 2016). Evidently, in Figure 7, the interpreted I_c for the same fly ash, which is a silt mixture, could switch from sand-like to clay-like behavior as a function of the penetration rate, showing uncertainties associated with soundings with partially drained conditions. In the current study, the F_r was kept constant. Thus, the I_c was dominated by the magnitude of Q_t, which further determined whether the fly ash exhibited a sand-like or clay-like behavior.

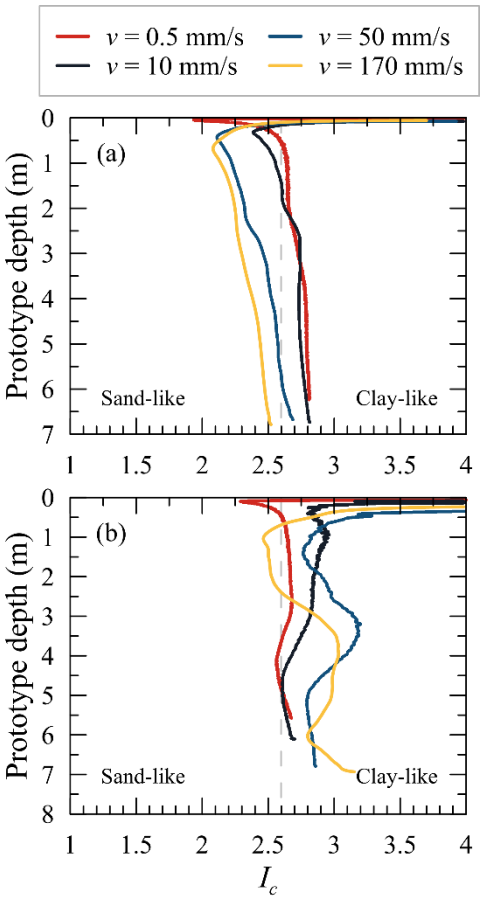

Figure 7. Interpreted soil behavior type index I_c profiles: (a) Test 1-1 (densest); (b) Test 1-2 (loosest).

An alternative interpretation of the soil behavior type, the modified soil behavior type index (I_B), was developed to overcome some of the aforementioned limitations of I_c (Robertson 2016). I_B can be calculated as follows:

$$I_B = 100(Q_{tn} + 10)/(70 + Q_{tn}F_r)^{0.5} \quad (10)$$

The resulting I_B profiles are shown in Figure 8. Similar to I_c, since the F_r was kept constant in the current study, the obtained I_B was driven by the magnitude of Q_{tn}. The I_B value successfully identified that the tested material is a transitional soil – silt mixture, as the calculated I_B using q_c under various penetration rates generally all fall in the

transitional soil region. The I_B interpreted using the drained q_c appears to be similar comparing Test 1-1 and 1-2 due to the similarity in the Q_{tn} magnitude. However, when the penetration rate increased and approached the undrained condition, Tests 1-1 and 1-2 exhibited different changes in I_B, where for the low void ratio test, the I_B shifted towards the sand-like region, and for the high void ratio test it shifted towards the clay-life region. This implies that the soil's undrained strength in Test 1-1 may resemble that of a coarse-grained soil, while the undrained strength of the soil in Test 1-2 resembles that of a fine-grained soil. The observation further emphasizes that comparing I_B profiles obtained from different penetration rates can inform the expected soil behavior.

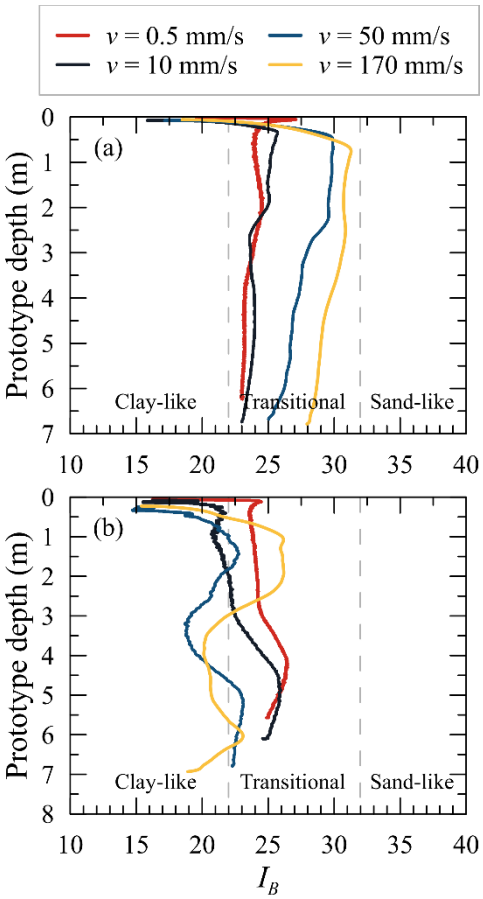

Figure 8. Interpreted modified soil behavior type index I_B profiles: (a) Test 1-1 (densest); (b) Test 1-2 (loosest).

4.4. Changes in Q_{tn} with penetration rate

According to the observation of the CPT profiles, the changes in cone tip resistance with penetration rate for fly ash deposits with different initial state provide insights into the volumetric change behavior of the soil. Further processing was conducted, and representative q_c and the corresponding Q_{tn} were obtained in each CPT sounding at a prototype depth of 5.5 – 6 m instead of at one specific depth to minimize the potential variations in the cone tip resistance, if any. The selected depth range was beyond the depth required to ensure deep penetration conditions in CPTs and fully mobilize the strength of the soil (Salgado 2014; Kim et al. 2016). Also, the representative depth range was determined such thatthe Q_{tn} values were relatively stablewith no abrupt change. The variation in the effective vertical stress in the depth range was small (41 – 52 kPa) and was caused by changes in the unit weight of the consolidated soil. In addition, Q_{tn} extracted in a depth range of 4.5 – 5 m are also ploted in Figure 9 (b) with low opacity for comparison. The values are similar to the ones in the depth range of 5.5 – 6 m. The $Q_{tn}/Q_{tn,undrained}$ plot (Figure 9 c) shows the same argument. The relationships between the representative cone tip resistance (q_c) and the normalized velocity V for all tests are illustrated in Figure 9 (a), while the relationship between Q_{tn} and V is shown in Figure 9 (b). Additionally, the Q_{tn} was normalized using the Q_{tn} obtained in the fastest pushes, which was assumed to be representative of undrained conditions (Figure 9 c). The q_c obtained using the slowest pushes (i.e., in drained conditions) was similar for the three models, consistent with the lack of an effect of density on the shear wave velocity (Figure 4). The changes in cone tip resistance (both q_c and Q_{tn}) with V generally show three different trends. q_c and Q_{tn} increased dramatically by a factor of over 2 in the densest model (Test 1-1), indicating a dilative tendency while approaching undrained conditions, during which negative porewater pressure was generated. q_c and Q_{tn} decreased by a factor up to about 1.5 in the loosest model (Test 1-2), indicating a contractive tendency while approaching undrained conditions, during which positive pore water pressure was generated. For intermediate model density (Test 1-4), the q_c and Q_{tn} generally changed little with the penetration rate. Thus, the overall change in q_c and Q_{tn} with V is concluded to be related to the void ratio of the fly ash, which provides confidence in using Q_{tn} values obtained at various drainage conditions to characterize the soil initial state.

4.5. State parameter evaluation

A more straightforward interpretation of the cone tip resistance under various drainage conditions is desired to facilitate an effective quantification of the state parameter, which is the key to characterizing soil behavior. Specifically, the pore water pressure generation is strongly tied to the soil volumetric change tendency of the soil during undrained loading. Robertson (2016) defined the boundary between the contractive and dilative (CD) behavior in the updated SBTn chart based on Q_{tn} and F_r. In the current study, with a F_r = 2.5%, a single Q_{tn} that separates the contractive and dilative behavior could be obtained, which ranges from 15 to 16, calculated based on:

$$CD = (Q_{tn} - 11)/(1 + 0.06F_r)^{17} \quad (11)$$

using CD = 70 (suggested boundary) and CD = 60 (lower bound). In Figure 9 (b), it is evident that the representative Q_{tn} from CPTs using the slowest two penetration rates (i.e., drained and partially drained) are close to the threshold Q_{tn} value, resulting in significant uncertainties in characterizing the soil behavior for the fly ash material tested. A closer evaluation of Tests 1-1 and 1-2 indicates that the soil behavior interpretation may span both TD (Transitional-Dilative) and TC (Transitional-Contractive) regions if different drainage

conditions are considered. The observation suggests that a single Q_{tn} could be insufficient to characterize the soil's volumetric tendencies in transitional silty soil that generates partially drained conditions at the standard penetration rate. Thereafter, an alternative parameter, $Q_{tn,drained}/Q_{tn,undrained}$, which quantifies the change in tip resistance as a result of a change in the drainage conditions and, thus, the magnitude of excess pore pressures, was adopted to develop an improved characterization framework.

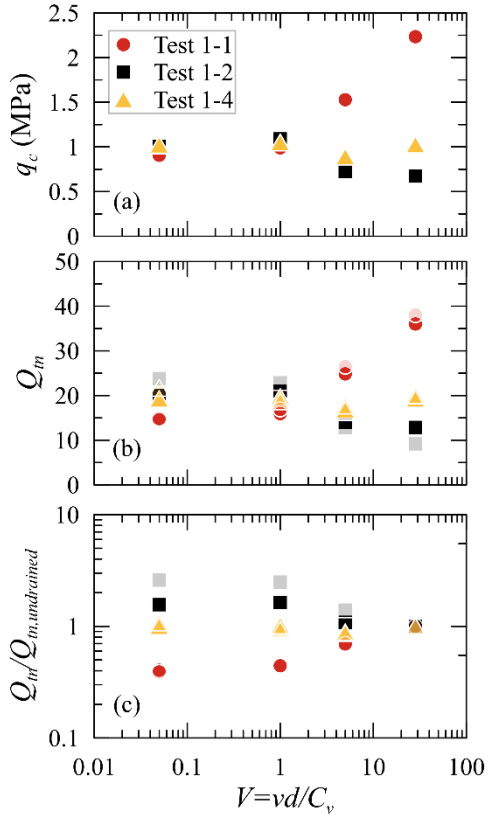

Figure 9. Changes in cone tip resistance with increasing normalized velocity: (a) cone tip resistance q_c; (b) overburden normalized cone tip resistance Q_{tn}; (c) ratio between Q_{tn} and the $Q_{tn,undrained}$ (datapoints with low opacity were extracted from a depth range of 4.5-5 m for comparison purposes only).

The $Q_{tn,drained}/Q_{tn,undrained}$ was found to be closely correlated to the model average void ratio, as shown in Figure 10 (a). The average void ratios reported are the mean values corresponding to the gravimetric water contents from the moisture sensor readings. The error bars in the figure represent the full range of the back-calculated void ratios. In addition, the standard deviation was calculated to be in the range of 0.026 – 0.059. Figure 10 (a) also includes data reported in EPRI (2021) to expand the range of average void ratio values, where the $Q_{tn,drained}/Q_{tn,undrained}$ were obtained at similar effective vertical stresses. The figure shows that as the average void ratio increases (i.e., as the model becomes looser), the $Q_{tn,drained}/Q_{tn,undrained}$ increases, indicating that the $Q_{tn,undrained}$ becomes increasingly smaller compared to $Q_{tn,drained}$ due to the generation of positive excess pore water pressure that softens the soil.

A similar relationship is presented in Figure 10 (b) with respect to the state parameter. The ψ values were obtained using the average void ratio, and the CSL presented in Eq. (2), assuming a K_o of 0.5 for the mean effective stress calculation. Similarly, the error bars represent the full range of the state parameter based on the moisture sensor readings. A deterministic relationship can be obtained using the average state parameter with respect to $Q_{tn,drained}/Q_{tn,undrained}$. This relationship has an exponential form and an $R^2 = 0.962$, as shown in the figure, with increasing $Q_{tn,drained}/Q_{tn,undrained}$ values as the ψ increases. Jefferies and Been (2015) pointed out that $\psi > -0.05$ is practically more effective for identifying soil with contractive volumetric change tendency. In Figure 10 (b), the findings in the current study reconcile with this argument that the models with a $\psi > -0.05$ exhibit $Q_{tn,drained}/Q_{tn,undrained}$ greater than 1, indicating a decrease in Q_{tn} under undrained conditions caused by positive excess pore water pressure generation.

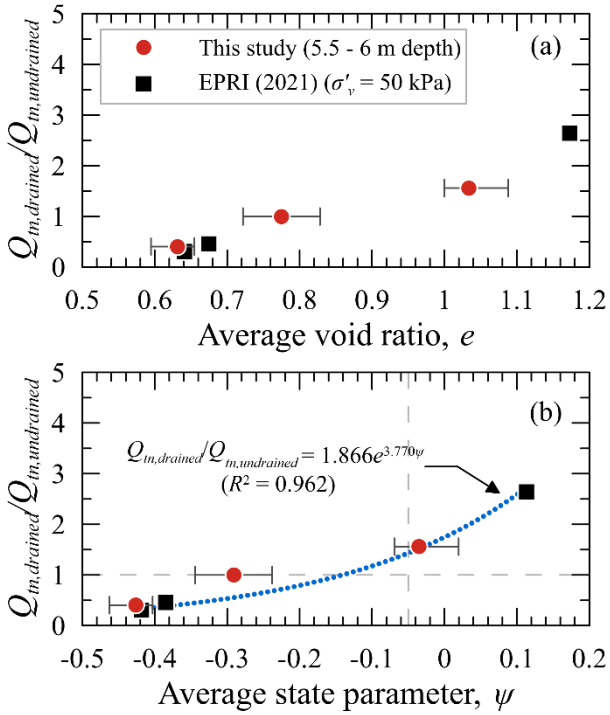

Figure 10. Relationship between the ratio between drained and undrained Q_{tn} and (a) average model void ratio and (b) average state parameter.

5. Conclusions

In-flight CPTs conducted with various penetration rates in geotechnical centrifuge models were used to aid in the characterization of soil behavior type, initial state, and volume change behavior of fly ash deposits. Instead of using one single push in the saturated fly ash deposits, a wide range of drainage conditions, spanning from the drained to partially drained and to the undrained condition, were mobilized using tests with different penetration rates. The obtained modified soil behavior type index I_B successfully identified the tested soil as a transitional soil. In addition, depending on the initial void ratio of the fly ash model, the cone tip resistance could increase, decrease, or stay relatively constant with an increasing penetration rate based on the material's volumetric change tendencies. The presented results demonstrated that the cone tip resistances at multiple

drainage conditions could be used to screen for dilative or contractile behavior. With further exploration, the $Q_{tn,drained}/Q_{tn,undrained}$ was found to be correlated with the initial void ratio and state parameter of the deposits, and an initial relationship is presented. However, this relationship is limited to a single material in a centrifuge environment. Further tests should be performed in different materials and in the field to verify the validity of a relationship between $Q_{tn,drained}/Q_{tn,undrained}$ and state parameter.

Acknowledgements

The authors are grateful for the financial support provided by the Electric Power Research Institute (EPRI).

References

ASTM. 2020. *D5778-20 Standard Test Method for Electronic Friction Cone and Piezocone Penetration Testing of Soils.* West Conshohocken, PA: ASTM.

Bachus, R. C., M. Terzariol, C. Pasten, S. H. Chong, S. Dai, M. S. Cha, S. Kim, J. Jang, E. Papadopoulos, S. Roshankhah, L. Lei, A. Garcia, J. Park, A. Sivaram, F. Santamarina, X. Ren, and J. C. Santamarina. 2019. "Characterization and Engineering Properties of Dry and Ponded Class-F Fly Ash." Journal of Geotechnical and Geoenvironmental Engineering, 145 no. 3 (Martch): 04019003. https://doi.org/10.1061/(ASCE)GT.1943-5606.0001986

Been, K., and M. G. Jefferies. 1985. "A state parameter for sands." Géotechnique, 35, no. 2 (February): 99–112. https://doi.org/10.1680/geot.1985.35.2.99.

Casagrande, A. 1936. "Characteristics of cohesionless soils affecting the stability of slopes and earth fills." J. Boston Society of Civil Engineers, 23, no. 1 (January): 13–32.

DeJong, J. T., and M. Randolph. 2012. "Influence of Partial Consolidation during Cone Penetration on Estimated Soil Behavior Type and Pore Pressure Dissipation Measurements." J. Geotech. Geoenviron. Eng., 138 no. 7 (July): 777–788. https://doi.org/10.1061/(ASCE)GT.1943-5606.0000646.

Dominguez-Quintans, C., J. a. H. Carraro, and L. Zdravkovic. 2023. "A Critical Assessment of the Effect of Initial Fabric on Key Small-Strain Design Parameters of Slurry-Deposited Silts and Sands." Journal of Geotechnical and Geoenvironmental Engineering, 149, no. 7 (July): 04023047. https://doi.org/10.1061/JGGEFK.GTENG-11305.

EPRI. 2021. *Geotechnical Centrifuge Tests to Assess Stability of Slurry-Deposited Coal Fly Ash: Runout and Dewatering Behavior Analysis.* Palo Alto, CA.

Jacobsz, S. W. 2018. "Low cost tensiometers for geotechnical applications." In *Physical Modelling in Geotechnics*. London: CRC Press.

Jefferies, M., and K. Been. 2015. *Soil Liquefaction: A Critical State Approach, Second Edition*. London: CRC Press.

Kim, J. H., Y. W. Choo, D. J. Kim, and D. S. Kim. 2016. "Miniature Cone Tip Resistance on Sand in a Centrifuge." J. Geotech. Geoenviron. Eng., 142, no. 3 (March): 04015090. https://doi.org/10.1061/(ASCE)GT.1943-5606.0001425.

Madabhushi, S. S. C., S. B. Follett, K. B. O'Hara, D. Wilson, B. L. Kutter, and A. Martinez. 2023. "Centrifuge Modeling of the Run-out behavior of Fly Ash Deposits Subjected to a Loss of Confinement." Can. Geotech. J. https://doi.org/10.1139/cgj-2022-0585.

Olson, S. M., and T. D. Stark. 2003. "Yield Strength Ratio and Liquefaction Analysis of Slopes and Embankments." J. Geotech. Geoenviron. Eng., 129, no. 8 (August): 727–737. https://doi.org/10.1061/(ASCE)1090-0241(2003)129:8(727).

Plewes, H. D., M. P. Davies, and M. G. Jefferies. 1992. "CPT based screen-ing procedure for evaluation liquefaction susceptibility." In *Proc., 45th Canadian Geotechnical Conf*, Toronto: Canadian Geotechnical Society.

Price, A. B., R. W. Boulanger, and J. T. DeJong. 2019. "Centrifuge Modeling of Variable-Rate Cone Penetration in Low-Plasticity Silts." J. Geotech. Geoenviron. Eng., 145, no. 11 (November): 04019098. https://doi.org/10.1061/(ASCE)GT.1943-5606.0002145.

Reid, D., R. Fanni, and A. Fourie. 2023. "A SHANSEP approach to quantifying the behaviour of clayey soils on a constant shear drained stress path." Can. Geotech. J. https://doi.org/10.1139/cgj-2022-0473.

Riveros, G. A., and A. Sadrekarimi. 2021. "Static liquefaction behaviour of gold mine tailings." Can. Geotech. J., 58, no. 6 (June): 889–901. https://doi.org/10.1139/cgj-2020-0209.

Robertson, P. K. 2010. "Evaluation of Flow Liquefaction and Liquefied Strength Using the Cone Penetration Test." J. Geotech. Geoenviron. Eng., 136, no. 6 (June): 842–853.

Robertson, P. K. 2016. "Cone penetration test (CPT)-based soil behaviour type (SBT) classification system — an update." Can. Geotech. J., 53, no. 12 (December): 1910–1927. https://doi.org/10.1139/cgj-2016-0044.

Salgado, R. 2014. "Experimental Research on Cone Penetration Resistance." In *Geo-Congress 2014 Keynote Lectures*, 140–163. Atlanta, Georgia: American Society of Civil Engineers.

Shuttle, D., and M. Jefferies. 2016. "Determining silt state from CPTu." Geotechnical Research, 3, no. 3 (March): 90–118.